

Article

A Study on Welding Deformation Prediction for Ship Blocks Using the Equivalent Strain Method Based on Inherent Strain

Yongtai Kim ¹, Jaewoong Kim ^{2,*} and Sungwook Kang ³ ¹ Ship Structure Research Department, Hyundai Heavy Industries, Ulsan 44032, Korea; yongtd@hhi.co.kr² Smart Manufacturing Process R&D Group, Korea Institute of Industrial Technology, Gwangju 61012, Korea³ Transport Machine Components R&D Group, Korea Institute of Industrial Technology, Jinju-si 52845, Korea; swkang@kitech.re.kr

* Correspondence: kjw0607@kitech.re.kr; Tel.: +82-63-600-6480

Received: 1 October 2019; Accepted: 8 November 2019; Published: 15 November 2019



Abstract: The welding process, which accounts for about 60% of the shipbuilding process, inevitably involves weld deformation. Considering this, productivity can be significantly increased if weld deformation can be predicted during the design phase, taking into account the fabrication order. However, the conventional welding deformation prediction method using thermo-elasto-plastic analysis requires a long analysis time, and the welding deformation prediction method using equivalent load analysis has a disadvantage in that the welding residual stress cannot be considered. In this study, an inherent strain chart using a solid-spring model with two-dimensional constraints is proposed to predict the equivalent strain. In addition, the welding deformation prediction method proposed in this study, the equivalent strain method (ESM), was compared with the ship block experimental results (EXP), elasto-plastic analysis (EPA) results, and equivalent load analysis (ELM) results. Through this comparison, it was found that the application of the equivalent strain method made it possible to quickly and accurately predict weld deformation in consideration of the residual stress of the curved double-bottom block used in the shipyard.

Keywords: welding deformation; welding residual stress; equivalent strain method; inherent strain method

1. Introduction

Ships are larger than regular transport structures, and thus their manufacturing process is more complex. Shipbuilding consists of multiple processes of assembling numerous members, materials, and equipment. This process starts with the design stage. The design stage proceeds in order of the initial, basic, detail, and production design. Steel plates are procured and processed after the design stage. The fabricated steel plates are used as members of the hull after the piece assembly process of attaching reinforcements to the inner structure of the hull and the sub-block assembly process of attaching frames to the outer plates of the hull. Then, the hull structure is assembled through the block assembly process. The ship is finally completed through the process of pre-outfitting, erection, and painting the outer plates of the hull.

Welding technologies are widely used in the production and assembly of ships. Steel hull welding is a complicated thermo-mechanical treatment process, because deformation and shrinkage of the materials are caused by the heat during the welding process. For this reason, skilled technicians spend a great deal of time and expense on the manual improvement process. Sometimes the deformation and shrinkage accumulate during the actual assembly stage, leading to situations where the gaps are too large to be welded in the block assembly stage.

As it takes a lot of time through simulations to calculate the shrinkage and deformation caused by welding large structures such as hull structures, several simple analysis methods have been developed over the years. It is necessary to calculate the deformation and shrinkage due to welding in the manufacturing stages quickly through simulations in advance. Based on the calculated welding deformation and shrinkage, this study aims to satisfy the allowable tolerances by offsetting the deformation and shrinkage in each assembly stage by providing accurate margins in the manufacturing stage.

In general, three methods are used to calculate weld deformation. The first is an experimental elasticity method, the second is a numerical method, and the third method is the equivalent load method. The development of these welding deformation methodologies is summarized in Table 1.

Table 1. Methodologies of welding deformation analysis.

	Period	Research Method	Researcher
Elasticity method	1950	Inherent strain theory	Watanabe et al. [1]
Numerical method	1960~	Finite element method, boundary element method	Masubuchi et al. [2]
Experimental-based	1980~	Calculates an equivalent loading using experimental data, elastic analysis	Ueda et al. [3] Nomoto et al. [4] Kim et al. [5]
Equivalent load method			Jang et al. [6,7] Kim et al. [8]
Inherent strain-based	1990~	Calculates an equivalent loading using inherent strain, elastic analysis	Murakawa et al. [9] Xiu et al. [10] Liang et al. [11] Kang et al. [12]

The elasticity method involves a simple welding experiment by changing the welding conditions and the dimensions of the work piece. After that, the factors affecting the welding deformation are summarized and the welding deformation is expressed using the equation for these factors. Watanabe et al. performed a study to obtain an analytical solution based on an elastic theory by applying strain to the initial state [1].

The numerical method, a thermal elasto-plastic analysis method, involves a simulation of all the physical phenomena relevant to the welding process that is as close to reality as possible. A numerical analysis is applied to the precise simulation of the welding process to determine the thermal, structural, and metallurgical phenomena. Masubuchi et al. applied the finite element method to the analysis of in-plane residual stresses in two-dimensional structures [2]. However, this requires a huge amount of computational time.

The equivalent load method extracts the characteristics of welding distortion and converts the sources of distortion into equivalent loads. This method can only be used to estimate the welding distortion of complicated structures in a very short time. The experimental-based equivalent load method was proposed by Ueda et al. and derived a moment equation that gave the same angular deformation as the experimental estimate [3]. Namoto et al. calculated equivalent load by arranging a correlation between angular deformation and heat input [4]. Kim et al. conducted an experiment to find the equivalent loads for the angular deformation and longitudinal bending of fillet welding [5].

The inherent strain method is the most suitable method for calculating the welding deformation and shrinkage in large structures such as hulls [6]. The inherent strain method involves a heat transfer analysis performed according to the welding conditions to predict the size of the heat-affected zone of the material, and then applies the inherent strain value to the corresponding area by substituting an elastic equivalent force to calculate the deformation of a structure. Here, inherent strain refers to permanent strains including plastic strain, thermal strain, and phase transformation strain. Jang et al. proposed a disk-spring model that used the strain-based equivalent load method for the analysis of three-dimensional structures [7]. Kim et al. calculated an inherent strain considering a temperature

gradient [8]. Murakawa et al. developed a model based on the inherent strain concept and iterative substructure method to calculate a large-scale welding problem [9]. Xiu et al. calculated the weld strain of the vacuum vessel using the inherent strain method [10]. In accordance with the thermal load conditions, a modified inherent strain method was applied to the 3D printing field [11] or friction stir welding field [12].

In this study, we propose an inherent strain method to efficiently calculate the welding deformation and shrinkage, considering the welding sequences, phase transformation, and natural convection with regard to the stiffened plates of the hull structure [13,14]. We calculated the welding deformation and residual stress of the stiffened curved plate by applying the method proposed in this study. This study also verified the validity of the proposed method by comparing the calculated welding deformation and residual stress with the experimental results under the same conditions. It is expected that the method proposed in this study can be applied to predicting the thermal deformation of plate forming by line heating [7], and line heating with the weaving motions [15] of curved plates.

2. Inherent Strain Due to Welding

The strain that causes permanent strain in a structure after welding is defined as inherent strain. When inherent stress is distributed as a continuum, the stress can be removed by separating the corresponding element from the continuum. It can be explained by the three-stage stress states as shown in Figure 1. Figure 1a is the continuum in the initial state where no stress exists. Figure 1b shows the stress distribution due to thermal strain. Figure 1c shows the stress relief by separating the element in the Figure 1b state. The residual strain of the separated element is referred to as the inherent strain, and is defined in Equation (1):

$$\varepsilon^* = \frac{ds_2 - ds_0}{ds_0}, \quad (1)$$

where ε^* is plastic strain, ds_2 is the length of an element in a stress-released state, and ds_0 is the initial length of an element.

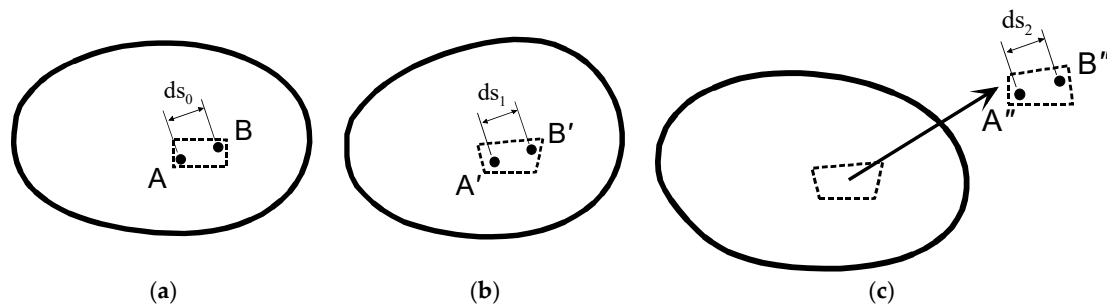


Figure 1. Definition of inherent strain: (a) initial state (stress free), (b) stressed state, (c) stress released state.

2.1. Calculation of the Inherent Strain

The inherent strain distribution can be formulated using a solid-spring model as shown in Figure 2. The welding region, where the inherent strain occurs, can be modeled as a solid and a spring.

In Figures 3–5, the values of inherent strain according to the maximum temperature and restraint were calculated using the solid-spring model. The solid-spring model has two different constraints: the x -direction constraint of the welding direction and the y -direction constraint of the direction perpendicular to the welding direction. The inherent strain was calculated by finite element method considering the temperature-dependent material properties [16] according to the highest temperature and the degree of restraint.

It was assumed that the degree of restraint in the x - and y -directions was the same as bead-on welding and the degree of restraint in the x -direction was 0.99 that of fillet welding. The inherent strain

chart was arranged with the x -axis of degree of restraint and the y -axis of inherent strain according to the highest temperature.

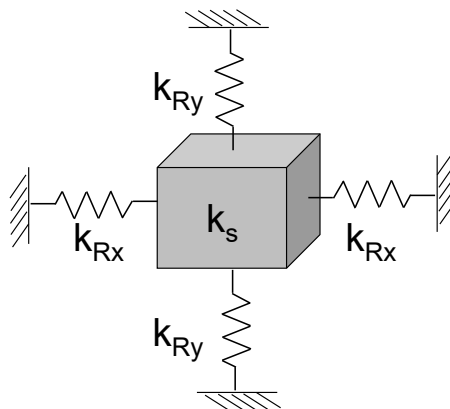


Figure 2. Solid-spring model.

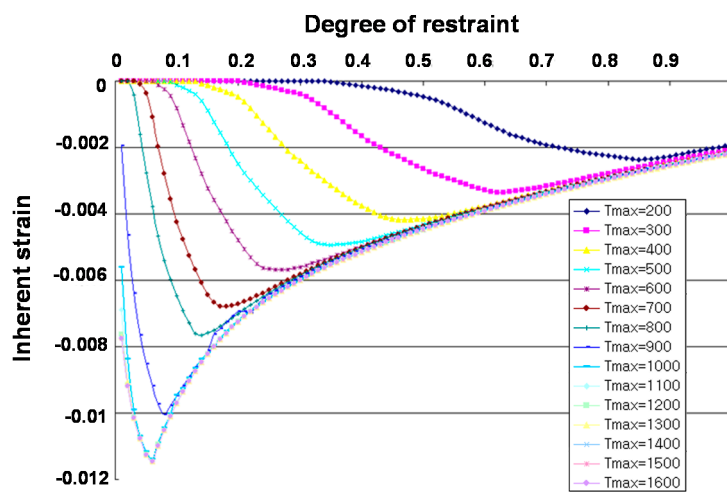


Figure 3. Inherent strain chart: butt welding.

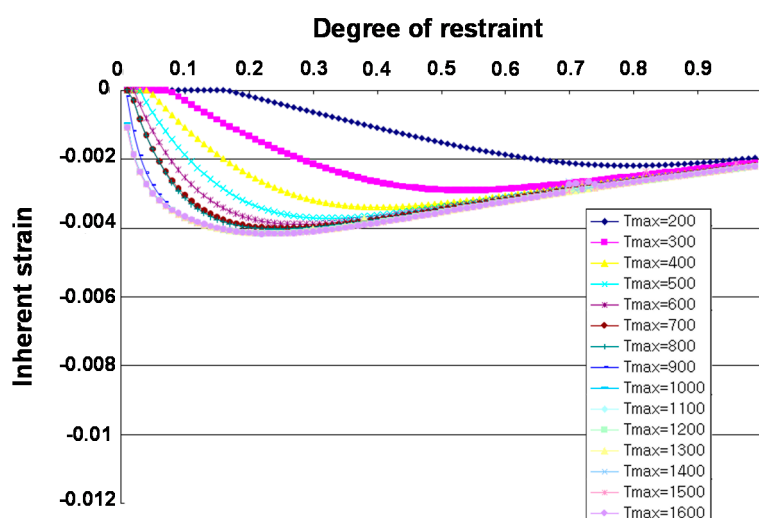


Figure 4. Inherent strain chart: fillet welding (y -direction).

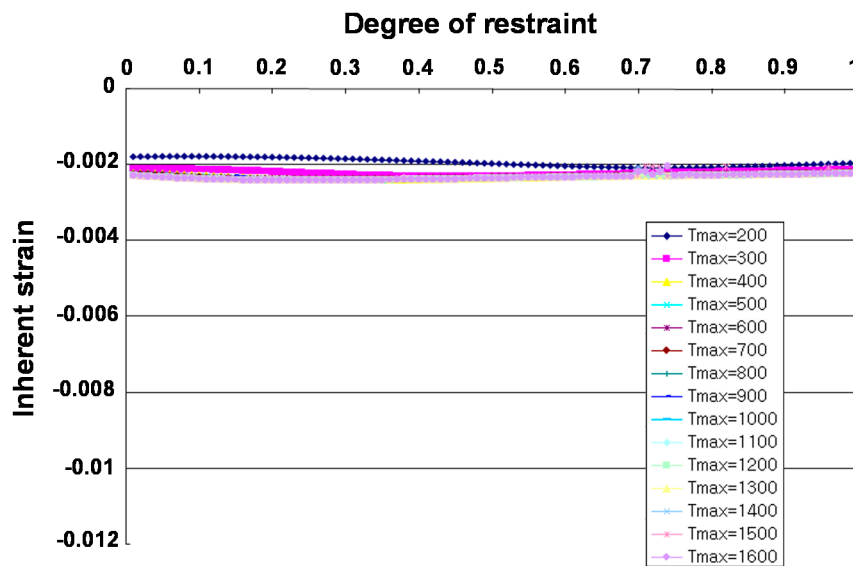


Figure 5. Inherent strain chart: fillet welding (x-direction).

2.2. Distribution of the Highest Temperature

The inherent strain is dependent on the highest temperature and the degree of restraint. Thus, the highest temperature of each node at the heat affected zone must be obtained to know the inherent strain. The heat source was modeled by a Gaussian model.

$$q(r) = q_{max} \exp(-\gamma r^2), \tag{2}$$

$$\int_0^{\infty} \int_0^{2\pi} q(r) r d\theta dr = \eta VI, \tag{3}$$

$$q_{max} = \frac{\gamma}{\pi} q_{eff}, \tag{4}$$

where $q(r)$ is heat flow input from the welding arc ($J/m^2 s$), q_{max} is heat flux at the center of arc ($J/m^2 s$), γ is the concentration coefficient (mm^{-2}), q_{eff} is the effective heat input rate (J/s), η is total arc efficiency, V is welding arc voltage (V), and I is welding arc current (A).

The highest temperature of each region was calculated by the two-dimensional FE heat transfer analysis as shown in Figure 6.

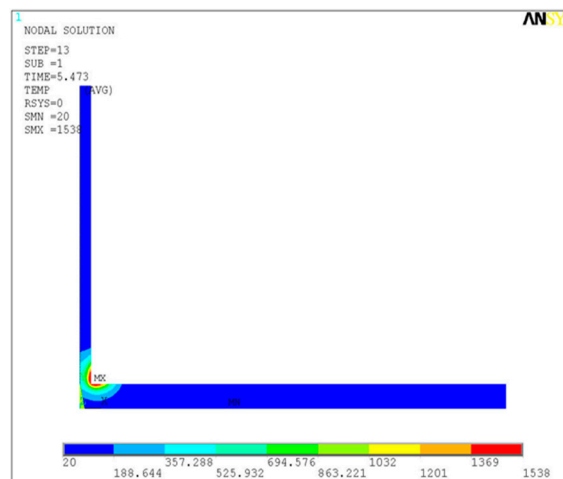


Figure 6. Heat transfer analysis (temperature distribution).

2.3. Calculation of Degree of Restraint

The degree of restraint indicates the level of resistance due to thermal deformation in the high-temperature zone during welding. The degree of restraint was determined by the stiffness of the solid and the spring, as shown in Figure 2, and can be expressed as Equations (5) and (6):

$$\beta_x = f(x, y, z) = \frac{k_{Rx}}{k_S + k_{Rx}}, \tag{5}$$

$$\beta_y = f(x, y, z) = \frac{k_{Ry}}{k_S + k_{Ry}}. \tag{6}$$

We needed to know the stiffness of the weld zone (high-temperature zone) and the periphery (low-temperature zone) to calculate the degree of restraint. To calculate the stiffness, this study performed an elastic analysis on the reinforcement plates with and without peripheries using the unit load method as shown in Figure 7. The unit load (P_u) was applied along the weld line at the end of the leg length of the weld for each thickness. We calculated the deformation according to the periphery, and finally calculated the stiffness of the weld zone and the periphery along the thickness direction.

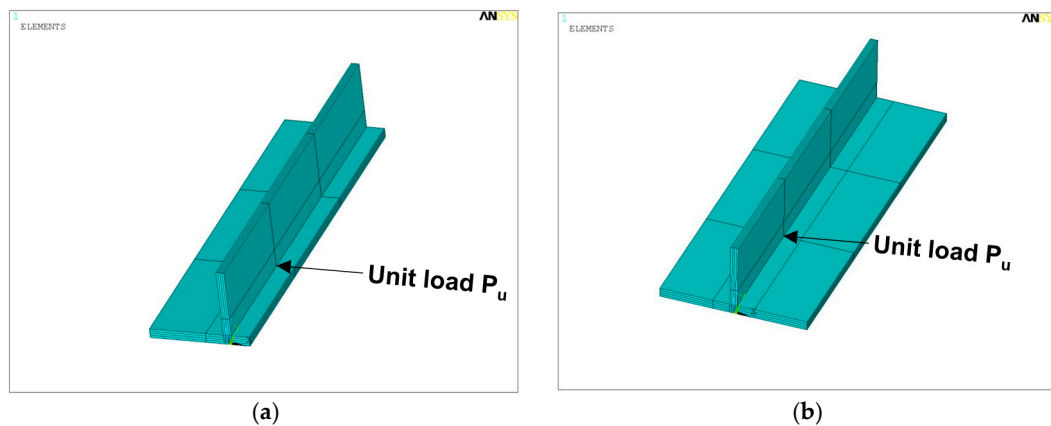


Figure 7. Degree of restraint of unit welding member: (a) without surrounding part, (b) with surrounding part.

The unit load P_u was applied at the end of the leg length of the weld on each layer, so the stiffness of the welding area and the surrounding area could be calculated:

$$k_S = \frac{P_u}{\delta_s}, \tag{7}$$

$$k_S + k_R = \frac{P_u'}{\delta_s'}, \tag{8}$$

where δ_s is the deformation when the external restraint is not considered, P_u' is the unit load when the external restraint is considered, and δ_s' is the deformation when the external restraint is considered.

When considering the welding sequence, it was necessary to calculate the degree of restraint at each welding stage. Using the degree of restraint of the welding area when the external restraint is not considered (β_f), the degree of restraint when the external restraint is considered (β_r) was calculated. It was assumed that the stiffness of the solid was equal at each welding stage.

$$\beta_f = \frac{K_{Sf}}{K_{Bf} + K_{Sf}} \tag{9}$$

$$K_{Sf} = \beta_f \times (K_{Bf} + K_{Sf}) = \beta_f \times R_f \tag{10}$$

$$K_{Bf} = R_f - K_{Sf} = (1 - \beta_f) \cdot R_f \tag{11}$$

$$\beta_r = \frac{K_{Sr}}{K_{Br} + K_{Sr}} \tag{12}$$

$$K_{Br} = K_{Bf} \text{ (Assumption)} \tag{13}$$

$$K_{Sf} = R_r - K_{Br} = R_r - K_{Bf} \tag{14}$$

3. Equivalent Strain Method

The inherent strain of every node in the inherent area was calculated by the inherent strain chart with the highest temperature and degree of restraint as shown in Figure 8. This inherent strain must be integrated for welding deformation analysis.

$$\bar{\varepsilon}_x = \frac{\sum \varepsilon_x \times dl}{L}, \tag{15}$$

where ε_{x_total} is the integrated inherent strain of the x layer and ε_x is the inherent strain of each node.

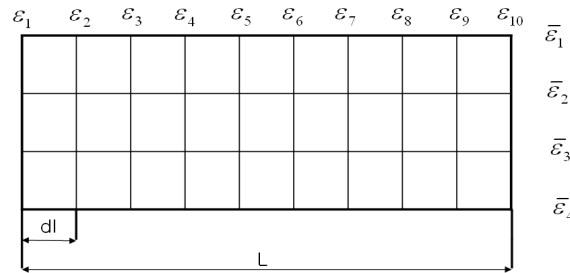


Figure 8. Calculation of the inherent strain.

The inherent strain was input by the equivalent thermal strain. A thermal expansion coefficient of 1 was assumed for user convenience. The inherent strain in the thickness direction was determined to satisfy the incompressibility condition.

$$\varepsilon_{res} = \alpha \Delta T = \Delta T \tag{16}$$

4. Welding Deformation Experiment

In this study, we performed a welding deformation experiment on four stiffened curved plates. Figure 9 shows the base plate and the stiffened plate used in the experiment. In terms of the shapes used in the experiment, we selected three different curvature models as shown in Figure 10 by investigating the members used in a shipbuilding yard ($\rho = 1000$ mm, 2000 mm, and 5000 mm, respectively). The welding constants included the girth length (1200 mm), breadth (800 mm), and the thickness of the base plate (16 mm).

The experiments were performed by changing only the welding sequence after applying the same curvature as shown in Figure 10b,c to examine the effect of the welding deformation on the welding sequence. In Figure 10b, the girder was welded after three longitudinal stiffeners were welded sequentially. In Figure 10c, the girder was welded first, then the remaining three longitudinal stiffeners were welded sequentially.

The experiment was conducted using an arc welding process to complete the final structure. The welding was performed at a voltage of 30 V, a current of 300 A, and a welding speed of 5 mm/s. Each weld was performed after air cooling under natural convection conditions.

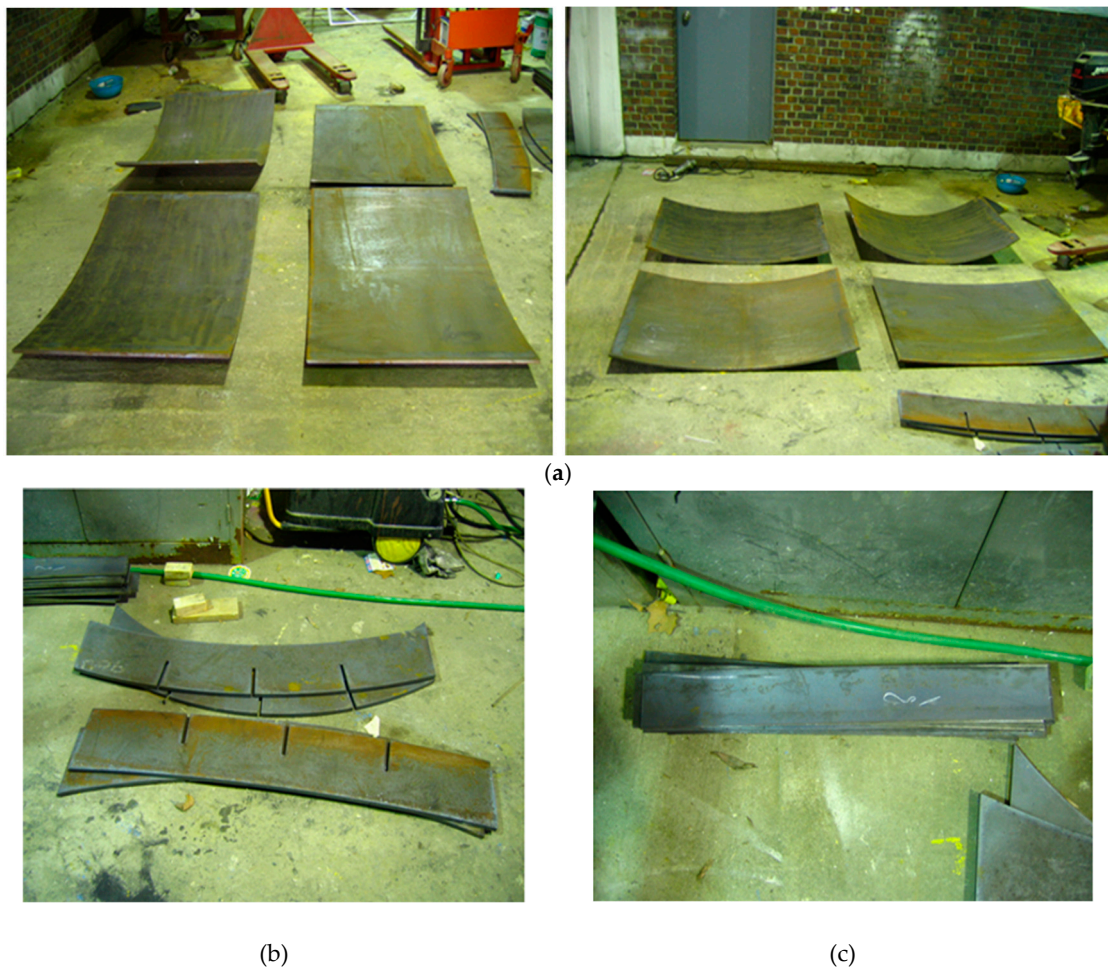


Figure 9. Plates and stiffeners for welding deformation: (a) base plates; (b) longitudinal stiffeners; (c) transverse stiffeners.

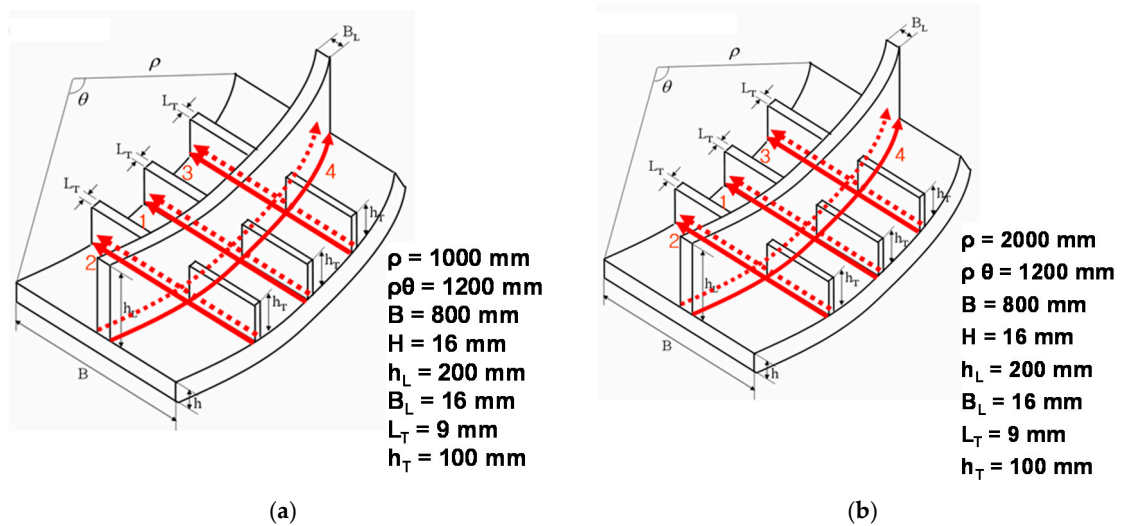


Figure 10. Cont.

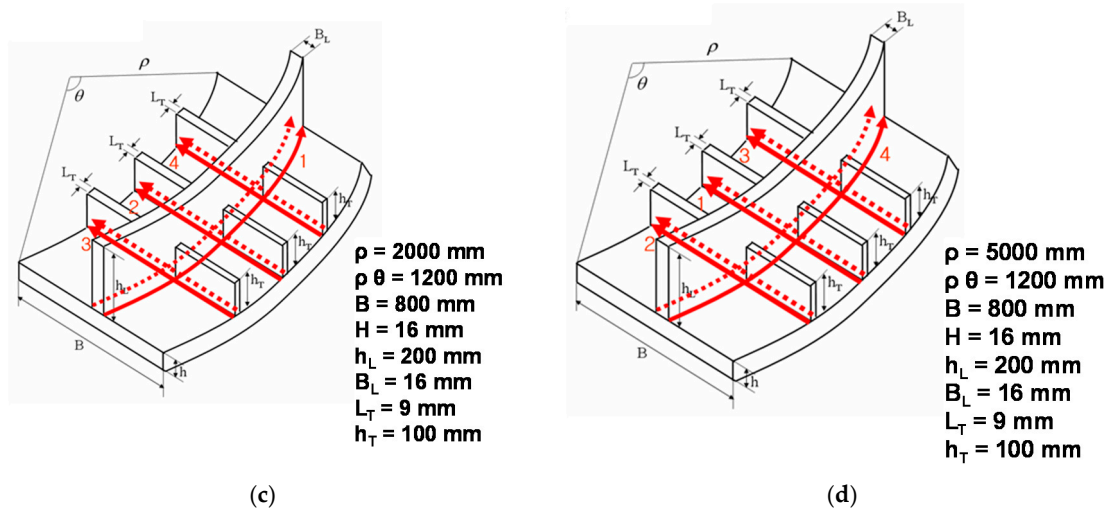


Figure 10. Experimental models with the welding sequences: (a) first experimental model: CASE 1; (b) second experimental model: CASE 2; (c) third experimental model: CASE 3; (d) fourth experimental model: CASE 4.

Figure 11 shows the welding operation and the structure after the welding.

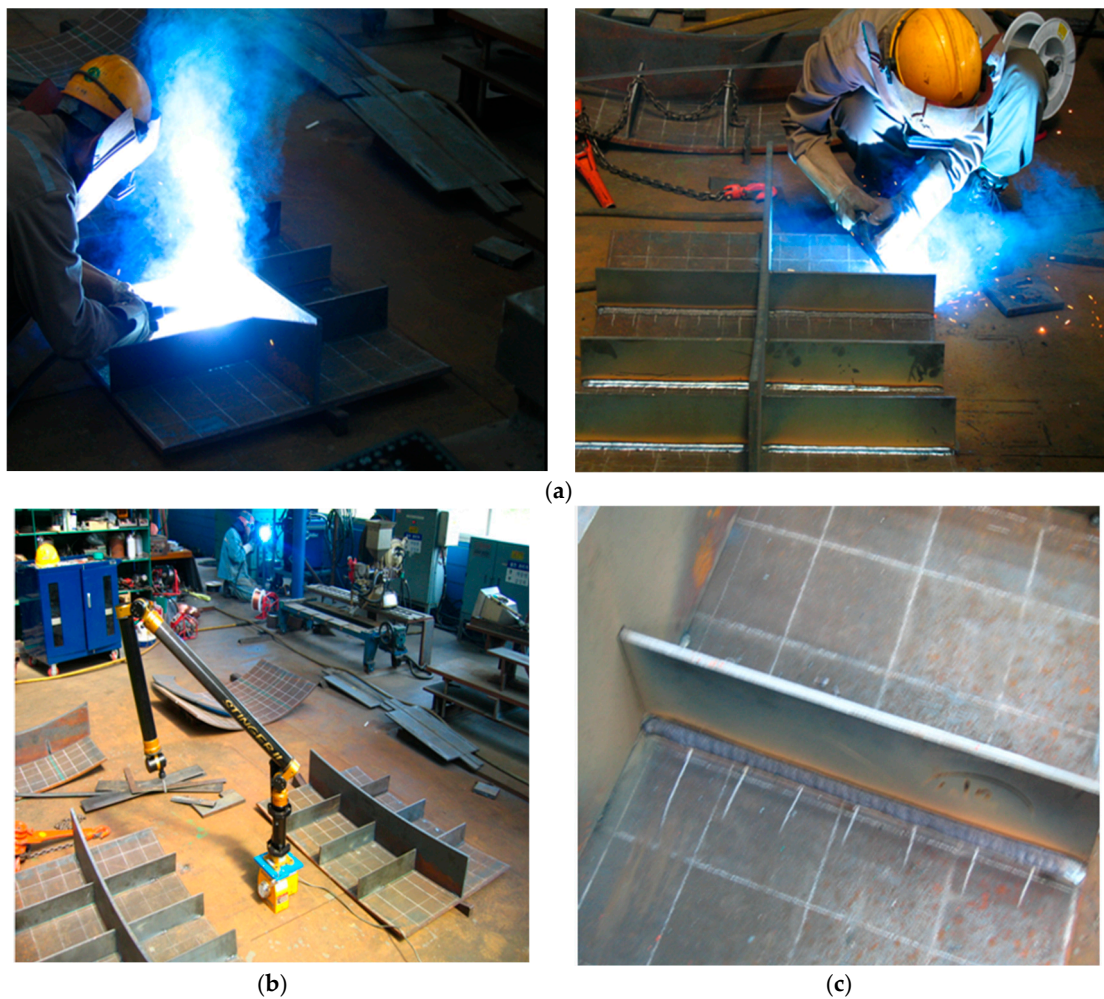


Figure 11. Experiments for welding deformation: (a) welding experiment, (b) structure after welding, (c) bead at the weld.

5. Comparison of Analysis and Experiment

In this study, thermal deformation analysis was performed using the shell element of the ANSYS program. The weld joint part was applied with 2 mm sized mesh, and the other structure parts were differentially applied with 5–20 mm mesh.

In the experiment, the grid was drawn at 100 mm intervals on the structure of the initial state and then marked at the vertex. Weld deformation was calculated by comparing the coordinates of the vertex, marking before and after welding using a three-dimensional measuring instrument.

The experimental result (EXP) was compared with three kinds of analyses as shown in Figure 12: elasto-plastic analysis (EPA), equivalent load method (ELM), and equivalent strain method (ESM).

In the case of the weld deformation analysis of the curved plate, the EPA showed the largest error with the experimental results, and inherent strain-based methods were similar to the experimental results.

In general, the welding deformation results of the EPA, ELM, and ESM are similar for simple structures. However, in this paper, welding deformation analysis was performed for complex structures with longitudinal and transverse stiffeners. In the case of the EPA, which considers material, geometry, and boundary condition nonlinearities, errors accumulated in the welding deformation analysis for complex structures. In addition, the elastic modulus decreased due to the increase of temperature at the nodes subjected to boundary conditions and this caused rigid body motion and increased errors in the EPA. When compared with the experimental results and the EPA results, the errors were larger than the ESM results as shown in Figure 12. However, the amounts of welding deformation in all three analysis methods (EPA, ELM, and ESM) were similar to the experimental results in terms of overall tendency. It was confirmed that the proposed method (ESM) was well suited for complex structures.

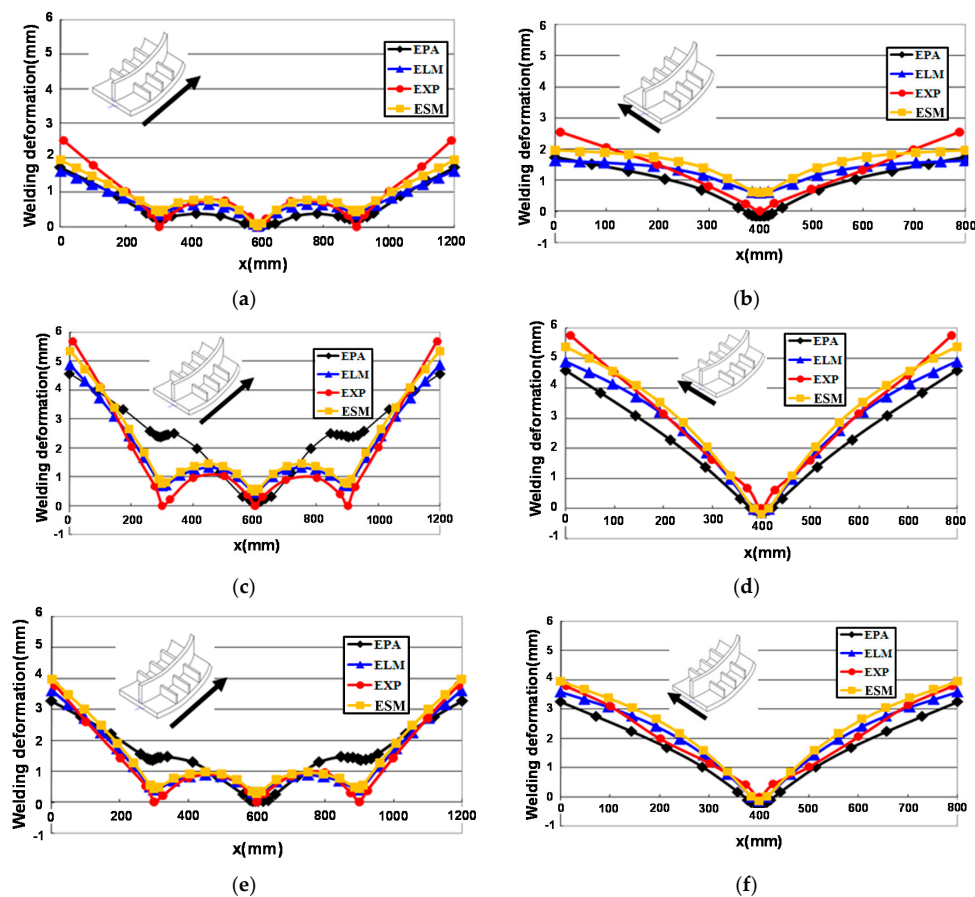


Figure 12. Cont.

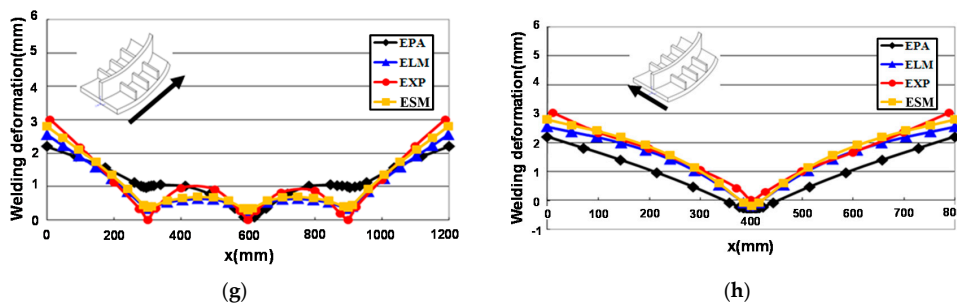


Figure 12. Comparison of welding deformations between experiment and analysis: (a) longitudinal direction (CASE 1), (b) transversal direction (CASE 1), (c) longitudinal direction (CASE 4), (d) transversal direction (CASE 4), (e) longitudinal direction (CASE 2), (f) transversal direction (CASE 2), (g) longitudinal direction (CASE 3), (h) transversal direction (CASE 3). EXP: experimental result; EPA: elasto-plastic analysis; ELM: equivalent load method; ESM: equivalent strain method.

6. Curved Double Bottom Block

The welding deformation analysis of the curved double bottom block using the equivalent strain method led to speculation about its application to actual ships.

The dimensions, welding sequence, and welding condition are shown in Table 2 and Figure 13.

Table 2. Dimensions and welding conditions.

	Size (mm)	Thickness (mm)	Heat Input (cal/mm)
Surface bottom	8000 × 7200, $\rho = 5000$	12	-
Inner bottom	8000 × 7200, $\rho = 5000$	12	-
Girder	8000 × 1200	12	252
Transverse Web	7200 × 1200	12	252
Longitudinal Stiffeners	8000 × 200	10	218.4

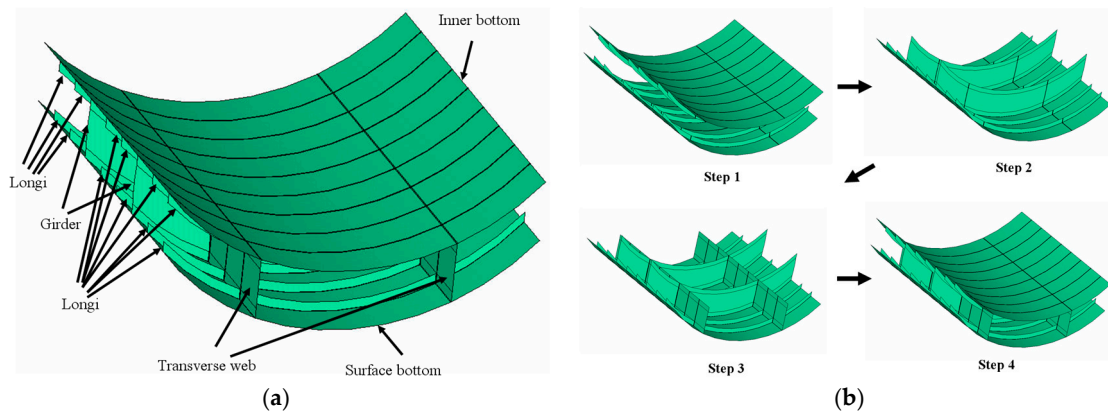
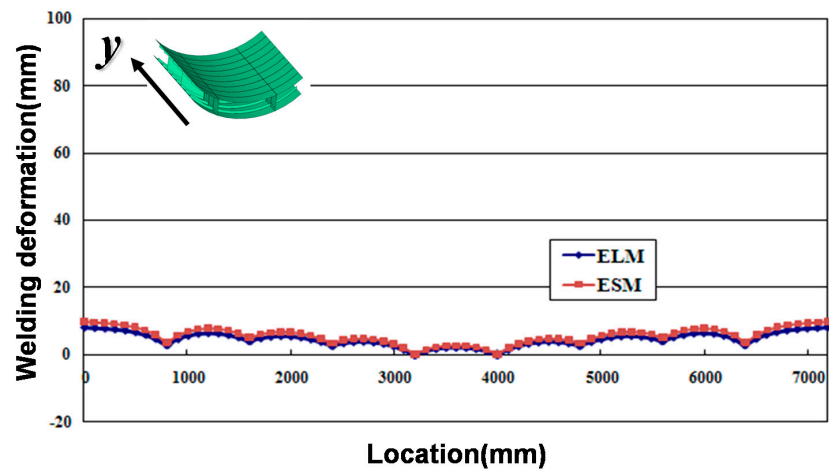
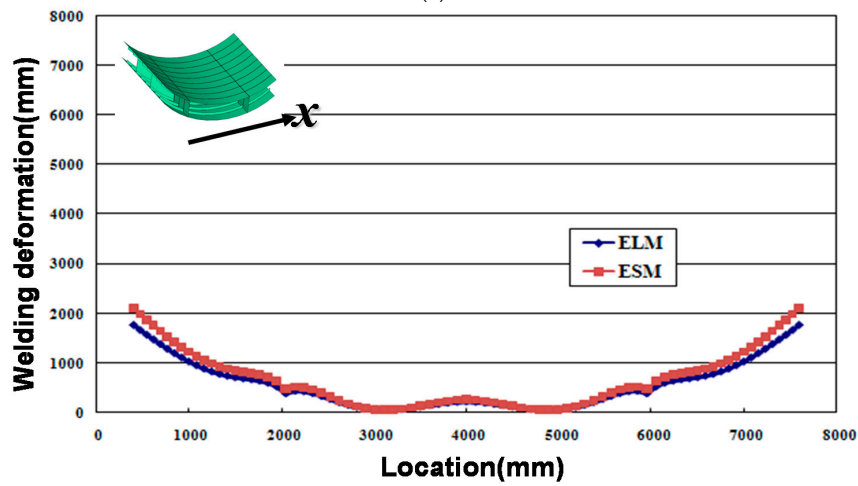


Figure 13. Analysis model: (a) curved double bottom block, (b) welding sequence.

The welding sequence was determined by considering the welding sequence in the shipyard. The result of an analysis of the curved double bottom block is shown in Figures 14 and 15.



(a)



(b)

Figure 14. Welding deformation of a curved double bottom block: (a) *y*-direction, (b) *x*-direction.

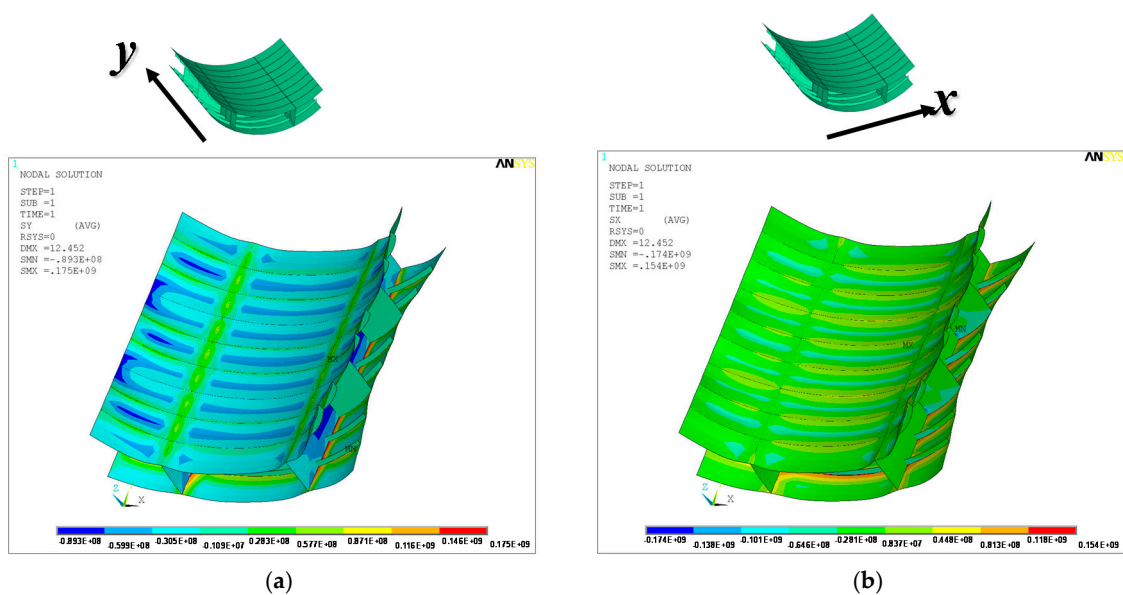


Figure 15. Stress distribution of a curved double bottom block: (a) *y*-direction, (b) *x*-direction.

The analysis results showed that the weld deformations of the ELM and the ESM were similar. In the case of the residual stress that was not calculated by the ELM, the ESM results confirmed that the weld showed the tensile residual stress distribution and the periphery showed the compressive residual stress distribution. This showed that it reflected the actual phenomenon well.

7. Analysis Time

Analysis times of the ESM, ELM, and EPA are compared in Table 3. The ESM and ELM were highly efficient compared with the EPA. Because the ESM could calculate residual stress, the ESM was a very powerful analysis method compared with the ELM.

Table 3. Comparison of analysis time.

	ESM	ELM	EPA
Analysis time (Experimental model)	2–3 (min)	1–2 (min)	1–2 (day)
Analysis time (Curved double bottom block)	15 (min)	7 (min)	Nearly impossible

8. Conclusions

This study proposed an efficient method for predicting welding deformation and residual stress using the equivalent strain method. We calculated the inherent strain value more accurately by proposing a solid-spring model that improved on the conventional bar-spring model. We were able to predict six general deformation modes of the structure generated during the welding process, and significantly reduced the analysis time compared to the thermal elasto-plastic analysis method. Through applying the proposed analysis method that used the welding sequence and curvature in the assembly stage as variables for the stiffened curved plate, the welding deformation and residual stress were found to be consistent with the experimental results.

As mentioned above, shipbuilding involves a process of assembling (mostly welding) complex members in a complicated sequence. Welding deformation and shrinkage are inevitable consequences of this process, and correcting them through straightening or modification involves a considerable amount of cost and time for skilled workers. The most efficient method to address these problems is to predict the deformation and residual stress according to the welding process conditions in advance and provide margins to the members. The method proposed in this study may be used to efficiently calculate the deformation and residual stress in the process of welding large structures such as in shipbuilding.

Author Contributions: Conceptualization, Y.K.; methodology, Y.K. and J.K.; software, Y.K. and S.K.; validation, Y.K. and J.K.; formal analysis, Y.K.; investigation, J.K. and S.K.; resources, Y.K. and J.K.; data curation, Y.K. and J.K.; writing—original draft preparation, Y.K.; writing—review and editing, Y.K. and S.K.; visualization, Y.K.; supervision, J.K.; project administration, Y.K. and J.K.; funding acquisition, Y.K. and J.K.

Funding: This study has been conducted with the support of the Korea Institute of Industrial Technology as “Study on the Optimal Welding Condition of Titanium Materials for Manufacturing Ship Scrubber (PJA19300)”.

Conflicts of Interest: The authors declare no conflict of interest.

References

1. Watanabe, M.; Satoh, K. Effect of Welding Conditions on the Shrinkage Distortion in Welded Structures. *Weld. J.* **1961**, *40*, 377–384.
2. Masubuchi, K.; Ich, N.T. Computer Analysis of Degree of Constraint of Practical Butt Joints. *Weld. J.* **1970**, *49*, 166–176.
3. Ueda, Y.; Yuan, M.G.; Tanigawa, M. New Measuring Method of 3-Dimensional Residual Stresses Based on Theory of Inherent Strain. *J. Soc. Naval Arch. Jpn.* **1979**, *145*, 203–211. (In Japanese) [[CrossRef](#)]

4. Takechi, S.; Aoyama, K.; Nomoto, T. Basic Studies on Accuracy Management System Based on Estimation of Weld Deformations. *J. Mar. Sci. Technol.* **1997**, *181*, 249–260.
5. Kim, S.I.; Lee, J.S. Development of Simple Prediction Method for Welding Distortion in Fillet Joints. *Proc. Annu. Spring Meet. Soc. Nav. Arch. Korea* **1996**, 265–270.
6. Jang, C.D.; Lee, C.H. Prediction of Welding Deformation of Stiffened Plates using inherent Strain Method. *Proc. Thirteen. Asian Tech. Exch. Advis. Meet. Mar. Struct.* **1999**, 485–492.
7. Jang, C.D.; Ko, D.E.; Seo, S.I. A Study on the Prediction of Deformations of Plates Due to Line Heating Using a Simplified Thermal Elasto-Plastic Analysis. *J. Ship Prod.* **1997**, *13*, 22–27.
8. Kim, T.J.; Jang, B.S.; Kang, S.W. Welding deformation analysis based on improved equivalent strain method considering the effect of temperature gradients. *Int. J. Nav. Arch. Ocean.* **2015**, *7*, 157–173. [[CrossRef](#)]
9. Murakawa, H.; Ma, N.; Huang, H. Iterative substructure method employing concept of inherent strain for large-scale welding problems. *Weld. World* **2015**, *59*, 53–63. [[CrossRef](#)]
10. Xiu, L.; Wu, J.; Liu, Z.; Ma, J.; Fan, X.; Ji, H.; Xia, X.; Li, Y. Weld distortion prediction of the CFETR vacuum vessel by inherent strain theory. *Fusion Eng. Des.* **2017**, *121*, 43–49. [[CrossRef](#)]
11. Liang, X.; Chen, Q.; Cheng, L.; Hayduke, D.; To, A.C. Modified inherent strain method for efficient prediction of residual deformation in direct metal laser sintered components. *Comput. Mech.* **2019**, 1–15. [[CrossRef](#)]
12. Kang, S.W.; Kim, J.W.; Jang, Y.J.; Lee, G.J. Welding Deformation Analysis, Using an Inherent Strain Method for Friction Stir Welded Electric Vehicle Aluminum Battery Housing, Considering Productivity. *Appl. Sci.* **2019**, *9*, 3848. [[CrossRef](#)]
13. Jang, C.D.; Ryu, H.S.; Lee, C.H. Prediction and Control of Welding Deformations in Stiffened Hull Blocks using Inherent Strain Approach. In Proceedings of the 14th ISOPE, Toulon, France, 23–28 May 2004; Volume 4, pp. 159–165.
14. Jang, C.D.; Ko, D.E.; Ha, Y.S. An Improved Inherent Strain Analysis for the Prediction of Plate Deformations Induced by Line Heating Considering Phase Transformation of Steel. *Int. Offshore Polar Eng. Conf.* **2003**, *17*, 147–152.
15. Jang, C.D.; Ha, Y.S.; Kim, Y.T. Determination of optimal heating conditions in line heating process with weaving motions. In Proceedings of the 16th ISOPE, San Francisco, CA, USA, 28 May–2 June 2006; Volume 5, pp. 182–186.
16. Lee, D.W. Thermo-Elasto-Plastic Modeling of GMAW Using the Finite Element Method. Ph.D. Thesis, Seoul National University, Seoul, Korea, 1995.



© 2019 by the authors. Licensee MDPI, Basel, Switzerland. This article is an open access article distributed under the terms and conditions of the Creative Commons Attribution (CC BY) license (<http://creativecommons.org/licenses/by/4.0/>).